Proceedings of ASME FEDSM'03
4th ASME/JSME Joint Fluids Engineering Conference
Honolulu, Hawaii, USA, July 6–10, 2003

FEDSM2003–45275

NUMERICAL MODELING OF FLUID TRANSIENTS BY A FINITE VOLUME PROCEDURE FOR ROCKET PROPULSION SYSTEMS

Alok K. Majumdar and Robin H. Flachbart
NASA Marshall Space Flight Center
Huntsville, Alabama USA

ABSTRACT

This paper describes the application of a finite volume procedure for a fluid network to predict fluid transients following a rapid valve closure in a long cryogenic pipeline. The conservation equations of mass, momentum, energy, and the equation of state for real fluids are solved in the fluid network consisting of nodes and branches. In the present formulation, the speed of sound does not appear explicitly in the governing equations. Instead, the equation of state for a real fluid is solved in conjunction with the conservation equations to calculate the compressibility factor for modeling the wave propagation phenomenon. The numerical procedure is also capable of modeling the wave propagation due to phase change and gas-liquid mixture. The predicted history of pressure and velocity variation in a single pipe has been compared to the solution by the method of characteristics (MOC) for liquid oxygen (LO_2), liquid hydrogen (LH_2), and water (H_2O). The paper also presents the numerical solution of pressure surges for a gas-liquid mixture, condensation of vapor, and flow circuit with parallel branches and tailpipe.

NOMENCLATURE

A	area (ft^2)
a	speed of sound (ft/s)
C_c	convergence criterion
$c_{i,k}$	mass concentration of kth specie at ith node
C_L	flow coefficient
C_p	specific heat at constant pressure (Btu/lb °F)
C_v	specific heat at constant volume (Btu/lb °F)
D	diameter (in)
f	friction factor
g_c	conversion constant (= 32.174 lb-ft/lb_f-s^2)
h	enthalpy (Btu/lb)
J	mechanical equivalent of heat (= 778 ft-lb_f/Btu)
K_f	flow resistance coefficient (lb_f-s^2/(lb-ft)^2)
L	length (in)
M	molecular weight
m	resident mass (lb)
$\dot{m}$	mass flow rate (lb/s)
N_E	number of iterations
N_{Re}	Reynolds number
n	number of branches connected to the ith node
n_f	number of fluids in a mixture
p	pressure (lb_f/ft^2)
R	gas constant (lb_f-ft/lb-R)
T	temperature (°F)
u	velocity (ft/s)
V	volume (ft^3)
x_v	vapor quality
x	mass fraction
$\bar{x}$	mole fraction
z	compressibility factor

Greek

Δ_{MAX}	normalized maximum correction
$\Delta\tau$	time step (s)
ε	surface roughness of pipe (in)
λ	period of oscillation
μ	viscosity (lb/ft-s)
ρ	density (lb/ft^3)
τ	time (s)
ϕ	density, specific heat, or viscosity

Subscript

i	node
ij	branch
k	specie
f, l	liquid
g, v	vapor
u	upstream

INTRODUCTION

Fluid transients, also known as water hammer, can have a significant impact on the design and operation of both spacecraft and launch vehicle propulsion systems. These transients often occur at system activation and shutdown. For ground safety reasons, many spacecraft are launched with the propellant lines dry. These lines are often evacuated by the time the spacecraft reaches orbit. When the propellant isolation valve opens during propulsion system activation, propellant rushes into the lines, creating a pressure surge. During propellant system shutdown, a pressure surge is created due to sudden closure of a valve. During both activation and shutdown, pressure surges must be predicted accurately to ensure structural integrity of the propulsion system fluid network.

The MOC is the most widely used method of calculating fluid transients in a pipeline [1–3]. In the MOC, two partial differential equations governing mass and momentum conservation equations

are combined into one ordinary differential equation which is then integrated by a finite difference procedure along the lines of characteristics. The time step is determined from the grid size and the speed of sound. The method is noniterative and possesses the accuracy of an analytical solution. Chaudhry and Hussaini [4] have used several predictor-corrector-based finite difference methods to calculate fluid transients. There has been, however, limited use of finite difference procedures based on MOC or a predictor-corrector scheme to model flow of the gas-liquid mixture or flow with cavitations. In recent years, a finite volume method has been developed [5] at NASA Marshall Space Flight Center (MSFC) to calculate network flow distribution in cryogenic systems for rocket engine applications. This method has been incorporated into a general-purpose computer program called the Generalized Fluid System Simulation Program (GFSSP) [6]. The GFSSP has been extensively validated by comparing its predictions with test data and other numerical methods for applications such as internal flow of the turbopump [7], propellant tank pressurization [8,9], and chill down of a cryogenic transfer line [10]. It is desirable that the code that has been used for calculating steady-state distribution as well as thermodynamic transients, such as tank blow down and pressurization for a given circuit, can also be used to investigate the effect of fluid transients, such as rapid valve closure and priming of evacuated feedlines. The purpose of this paper is to investigate the applicability of the finite volume method incorporated in the GFSSP to predict fluid transients in flow circuits.

MATHEMATICAL FORMULATION AND SOLUTION PROCEDURE

Finite Volume Formulation in a Fluid Network

Figure 1 shows a long pipeline connected to a tank. An isolation valve is placed at the end of the pipeline. The pipeline is discretized into nodes that are connected by branches as shown in Figure 2a. The branches are segments of pipeline that can be compared with "reaches" of the MOC. The discretization scheme assumes that the flow is driven by the pressure differential between the upstream and downstream nodes. This is known as the "staggered grid" technique that is commonly used in solving Navier-Stokes equations by the finite volume method [11].

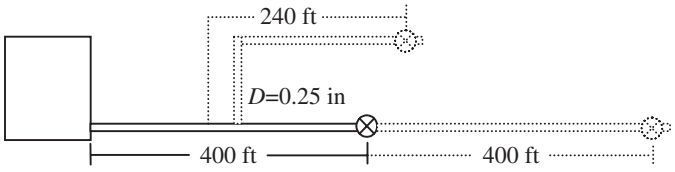

Figure 1. Schematic of the propellant tank, pipeline, and valve; solid line represents test cases 1–9 and dashed line represents test case 10 (Table 1).

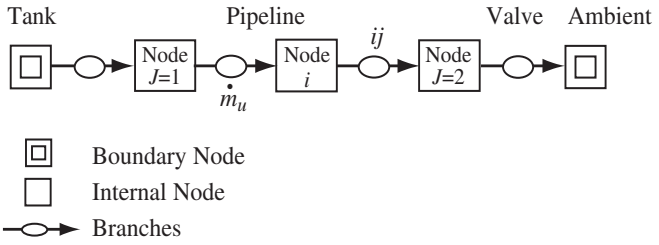

Figure 2a. Network flow model of the fluid system consisting of a tank, pipeline, and valve constructed with boundary nodes, internal nodes, and branches.

The nodes are of two kinds: boundary and internal nodes. At the boundary nodes, pressure and temperature is specified. At the internal nodes, all scalar properties such as pressure, temperature, density, compressibility factor, and viscosity are computed. Mass and energy conservation equations are solved at the internal nodes in conjunction with the thermodynamic equation of state. Flow rates are computed at the branches by solving the momentum conservation equation.

Figure 2b shows the finite volume model of the pipe. The model consists of 12 nodes and 11 branches. Node 1 is a boundary node representing the propellant tank. The pressure, temperature, and concentrations, if applicable, are prescribed at node 1. Node 12 is also a boundary node representing the ambient condition. Nodes 2 to 11 are internal nodes where pressure and temperature are computed. The first 10 branches (12 to 1011) represent pipe segments each of 40 ft in length. Branch 1112 represents the valve.

Mass Conservation. The mass conservation equation at the *i*th node can be written as

$$\frac{m_{\tau+\Delta\tau}-m_{\tau}}{\Delta\tau}=-\sum_{j=1}^{j=n}\dot{m}_{ij} \tag{1}$$

Equation (1) implies that the net mass flow from a given node must equate to the rate of change of mass in the control volume. In the steady-state formulation, the left side of the equation is zero, such that the total mass flow rate into a node is equal to the total mass flow rate out of the node.

Momentum Conservation. The momentum conservation equation at the *ij* branch can be written as

$$\frac{(mu)_{\tau+\Delta\tau}-(mu)_{\tau}}{g_c\Delta\tau}+\mathrm{MAX}\left|\dot{m}_{ij},0\right|\left(u_{ij}-u_u\right)-\mathrm{MAX}\left|-\dot{m}_{ij},0\right|\left(u_{ij}-u_u\right)$$
$$=\left(p_i-p_j\right)A_{ij}-K_f\dot{m}_{ij}\left|\dot{m}_{ij}\right|A_{ij} \tag{2}$$

The left-hand side of the momentum equation contains the unsteady and inertia term. The pressure and friction force appear on the right-hand side of the equation. The unsteady term represents rate of change of momentum with time. For steady-state flow, the time step is set to an arbitrary large value and this term is reduced to zero. The inertia term is important when there is a significant change in velocity in the longitudinal direction due to change in area and density. An upwind differencing scheme is used to compute the velocity differential. The pressure term represents the pressure gradient in the branch. The pressures are located at the upstream and downstream face of a branch. Friction was modeled as a product of K_f and the square of the flow rate and area. It may be noted that $\dot{m}_{ij}\left|\dot{m}_{ij}\right|$ has been used instead of $\dot{m}_{ij}^2$. Recognizing the flow rate is a vector quantity, this technique is used to ensure that friction always opposes the flow. K_f is a function of the fluid density in the branch and the nature of the flow passage being modeled by the branch. For a pipe, K_f can be expressed as

$$K_f=\frac{8fL}{\rho_u\pi^2D^5g_c} \tag{3}$$

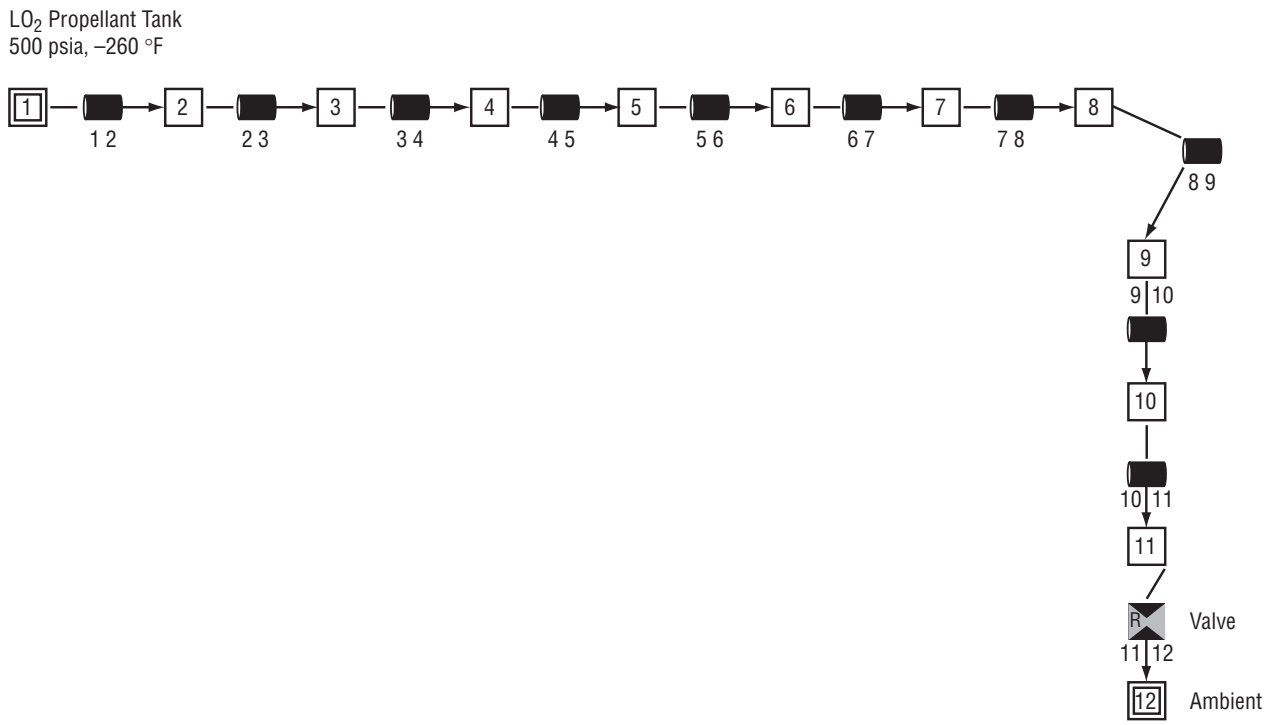

Figure 2b. Finite volume model of the flow network with a single pipeline and a valve.

For a valve, K_f can be expressed as

$$K_f = \frac{1}{2 g_c \rho_u C_L^2 A^2} \tag{4}$$

The friction factor, f, in Eq. (3) is calculated from the Colebrook equation [12], which is expressed as

$$\frac{1}{\sqrt{f}} = -2 \log\left[\frac{\varepsilon}{3.7D} + \frac{2.51}{N_{Re}\sqrt{f}}\right] \tag{5}$$

Energy Conservation. The energy conservation equation for node i, shown in Fig. 2, can be expressed following the first law of thermodynamics using enthalpy as the dependant variable. The energy conservation equation based on enthalpy can be written as

$$\frac{m\left(h - \frac{p}{\rho J}\right)_{\tau+\Delta\tau} - m\left(h - \frac{p}{\rho J}\right)_{\tau}}{\Delta\tau} = \sum_{j=1}^{j=n} \left\{ \mathrm{MAX}\left[-\dot{m}_{ij}, 0\right] h_j - \mathrm{MAX}\left[\dot{m}_{ij}, 0\right] h_i \right\} \tag{6}$$

The rate of increase of internal energy in the control volume is equal to the rate of energy transport into the control volume minus the rate of energy transport from the control volume. The MAX operator represents the upwind formulation.

Equation of State. The resident mass in the ith control volume can be expressed from the equation of state for a real fluid as

$$m = \frac{pV}{RTz} \tag{7}$$

For a given pressure and enthalpy, the temperature and compressibility factor in Eq. (6) is determined from the thermodynamic property program developed by Hendricks et al. [13,14].

Gas Liquid Mixture. To model a homogeneous mixture of liquid and gaseous species are solved in conjunction with Eqs. (1), (2), and (7). The conservation equation of the kth specie can be written as

$$\frac{\left(m_i c_{i,k}\right)_{\tau+\Delta\tau} - \left(m_i c_{i,k}\right)_{\tau}}{\Delta\tau} = \sum_{j=1}^{j=n} \left\{ \mathrm{MAX}\left[-\dot{m}_{ij}, 0\right] c_{j,k} - \mathrm{MAX}\left[\dot{m}_{ij}, 0\right] c_{i,k} \right\} \tag{8}$$

Unlike a single fluid, the energy equation for a gas-liquid mixture is expressed in terms of temperature instead of enthalpy:

$$\left(T_i\right)_{\tau+\Delta\tau} = \frac{\sum_{j=1}^{j=n} \sum_{k=1}^{k=n_f} Cp_k\, x_k T_j\, \mathrm{MAX}\left[-\dot{m}_{ij}, 0\right] + \left(C_{v,i} m_i T_i\right)_{\tau} / \Delta\tau}{\sum_{j=1}^{j=n} \sum_{k=1}^{k=n_f} Cp_k\, x_k \mathrm{MAX}\left[\dot{m}_{ij}\right] + \left(C_{v,i} m\right)_{\tau} / \Delta\tau} \tag{9}$$

It is assumed that the liquid and gas have the same temperature; however, specific heat of liquid and gas are evaluated from a thermodynamic property program [13]. The density, specific heat, and viscosity of the mixture are then calculated from the following relations:

$$\rho = \frac{p_i}{\sum_{k=1}^{k=n_f} [\bar{x}_k R_k] \sum_{k=1}^{k=n_f} [\bar{x}_k z_k] T_i} \tag{10}$$

where

$$z_k = \frac{p_i}{\rho_k R_k T_i} \tag{11}$$

$$C_v = \frac{\sum_{k=1}^{k=n_f} \bar{x}_k C_{v,k} M_k}{\sum_{k=1}^{k=n_f} \bar{x}_k M_k} \tag{12}$$

$$\mu_i = \sum_{k=1}^{k=n_f} \bar{x}_k \mu_k \tag{13}$$

Phase Change. Modeling phase change is fairly straightforward in the present formulation. The vapor quality of saturated liquid vapor mixture is calculated from

$$x_v = \frac{h - h_f}{h_g - h_f} \tag{14}$$

Assuming a homogeneous mixture of liquid and vapor, the density, specific heat, and viscosity are computed from the following:

$$\phi = (1 - x_v)\phi_l + x_v \phi_v \tag{15}$$

where ϕ represents density, specific heat, or viscosity.

Solution Procedure

The pressure, enthalpy, and resident mass in internal nodes and flow rate in branches are calculated by solving Eqs. (1), (6), (7), and (2), respectively. For a mixture, the conservation of species (Eq. (8)) is solved in conjunction with Eqns. (1), (7), and (2). The energy equation is solved in terms of temperature (Eq. (9)) instead of enthalpy. A combination of the Newton-Raphson method and the successive substitution method has been used to solve the set of equations. Mass conservation, momentum conservation, and resident mass equations (Eqs. (1), (2), and (7), respectively) are solved by the Newton-Raphson method. The energy and specie conservation equations are solved by the successive substitution method. The temperature, density, and viscosity are computed from pressure and enthalpy using a thermodynamic property program [13,14]. Figure 3 shows the flow diagram of the simultaneous adjustment with successive substitution scheme. The iterative cycle is terminated when the normalized maximum correction, Δ_{MAX}, is less than the convergence criterion, C_c. Δ_{MAX} is determined from

$$\Delta_{MAX} = \text{MAX} \left| \sum_{i=1}^{N_E} \frac{\phi_i'}{\phi_i} \right| \tag{16}$$

The convergence criterion is set to 0.001 for all models presented in this paper. The details of the numerical procedure are described in References [5] and [6].

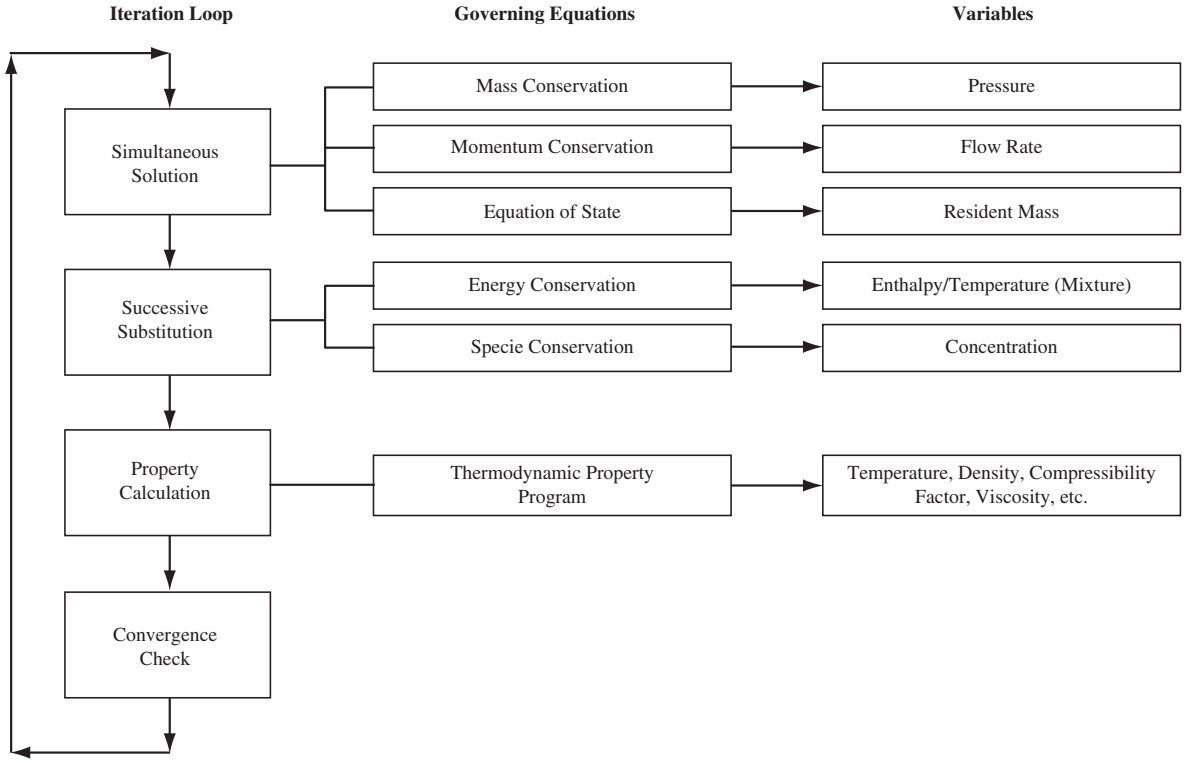

Figure 3. Simultaneous adjustment with successive substitution scheme for solving governing equations.

RESULTS AND DISCUSSION

The GFSSP model of the propellant tank and pipeline schematic is shown in Fig. 1. The valve closes in 0.1 s, which is considered rapid closure since the valve closure time is less than the period of oscillation, $2L/a$, where L is the length of the tube and a is the speed of sound.

Description of Test Cases

Several test cases are used to verify and investigate the applicability of the proposed method to predict fluid transient. The test cases presented in this paper are shown in Table 1. The purpose of test cases 1–3 is to investigate the effect of the number of branches on the solution. The numerical solutions were obtained for the same boundary condition and geometry with 5 branches (case 3), 10 branches (case 1), and 20 branches (case 2). Different fluids, namely H_2O and LH_2, are used in test cases 4 and 5. A mixture of LO_2 and gaseous helium (GHe) has been considered in test cases 6 and 7. Test cases 8 and 9 demonstrate the wave propagation due to condensation. A more complex flow circuit consisting of a network with two branches has been considered in test case 10. The time step for each test case is so chosen that the Courant number ($= L_{Branch}/(a\times\Delta\tau)$ is less than unity.

Comparison of MOC and Grid Sensitivity

Comparison of predicted pressures between the MOC and finite volume solution for three fluids (water, oxygen, and hydrogen) is shown in Table 2 and Figure 4. Figure 5 shows the grid sensitivity of finite volume solution. It is observed that there is a perfect agreement for the period of oscillation between two methods. Both solutions are also in agreement with the characteristic wavelength equation expressed as ($\lambda = 4L/a$) where λ is the period of oscillation. Maximum pressure predicted by two methods compares reasonably well. With grid refinement, the GFSSP solution of maximum pressure tends to approach the MOC solution. Discrepancies, however, are observed between the two methods in damping rate and shape of the curve. These are largely due to the way the physics of the flow was modeled in two different methods. For example, MOC uses speed of sound in the governing equation, while in the present formulation, the effect of speed of sound is modeled by the compressibility factor, which is computed from the energy equation and the equation of state. In addition, the valve closure history has not been perfectly matched between the two solutions, because different time steps were used in two solutions.

Nevertheless, the overall agreement with the MOC solution establishes the viability of the finite volume method to predict the fluid transient for design of the propulsion system fluid network.

Table 1. Description of test cases.

Case No.	Fluid	No. of Branches (Reaches)	Time Step (s)	Speed of Sound (ft/s)	Flow Rate (lb/s)	p_{max} (psia)	Period of Oscillation (s)
1	LO_2	10	0.01	2462	0.0963	626	0.65
2	LO_2	20	0.005	2462	0.0963	632	0.65
3	LO_2	5	0.02	2462	0.0966	620	0.65
4	H_2O	10	0.005	4874	0.071	704	0.33
5	LH_2	10	0.005	3725	0.0278	545	0.43
6	LO_2 and GHe (0.1% by mass)	10	0.01	1290**	0.0963	580	1.24
7	LO_2 and GHe (0.5% by mass)	10	0.01	769**	0.0963	520	2.08
8*	LO_2 (2 phase) $x_{exit} = 0.017$	10	0.01	–	0.0963	550	1.17
9*	LO_2 (2 phase) $x_{exit} = 0.032$	10	0.01	–	0.0963	538	1.22
10	LO_2	–	0.01	2462	0.0963	611	0.65

* Pressure oscillations are due to condensation
** Estimated from period of oscillation ($a=4L/\lambda$)

Table 2. Comparison between GFSSP and MOC solution.

Fluid	Flow Rate (lb/s)	Velocity (ft/s)	Friction Factor (Used in MOC Solution)	Speed of Sound (ft/s)	Max. Pressure Rise Above Supply Pressure (psi)		Period of Oscillation (s)	
					MOC	GFSSP	MOC	GFSSP
H_2O	0.071	3.34	0.0347	4892	214	204	0.33	0.33
LO_2	0.0963	4.35	0.0196	2455	136	126	0.65	0.65
LH_2	0.0278	19.01	0.0157	3725	61	45	0.43	0.43

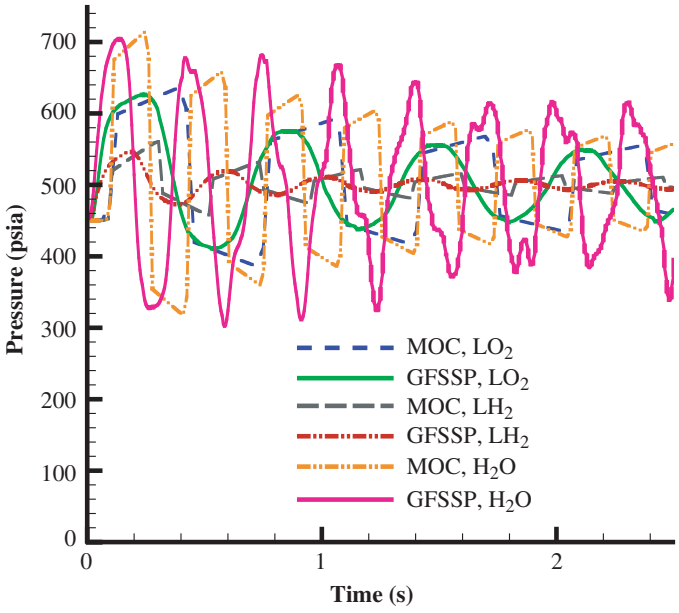

Figure 4. Comparison of pressure history between finite volume (GFSSP) and MOC solution for the three fluids (test cases 1, 4, and 5).

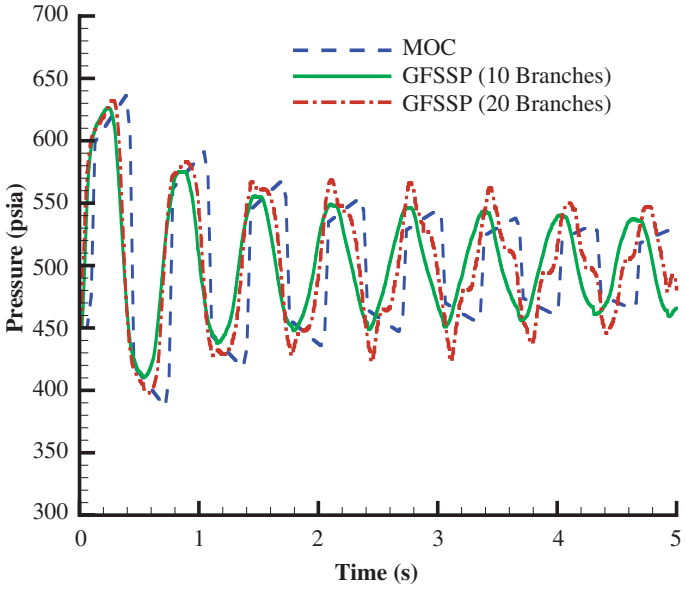

Figure 5. Predicted pressure by MOC and finite volume (GFSSP) methods (test cases 1 and 2).

Gas-Liquid Mixture

Test cases 6 and 7 demonstrate the capability of modeling a gas-liquid mixture. It is assumed that the tank supplies a mixture of LO_2 and GHe. The downstream pressure was adjusted until the flow rate nearly matches case 1. With the identical valve closure sequence and 0.1% by mass GHe, the peak pressure decreases from 626 to 580 psia and the period of oscillation increases from 0.65 to 1.24 s. Figure 6 shows the comparison of predicted pressure history for test cases 1, 6, and 7. With 0.5% by mass GHe, the peak pressure drops to 520 psia and the period of oscillation increases to 2.08 s. With the presence of GHe, the compressibility increases; therefore, peak pressure decreases.

Condensation

Wave propagation due to condensation is modeled in test cases 8 and 9. In these two test cases, the tank temperature is raised to –202 °F and –201 °F, respectively. The intent is to have a saturated flow, consisting of liquid and vapor, near the exit of the pipe. In test cases 8 and 9, the vapor mass fraction (quality) at the pipe exit was 0.012 and 0.025, respectively. The flow behavior for a liquid vapor mixture is quite different from single-phase flow, as can be seen in Figure 7. In these cases, pressure does not start oscillating immediately after valve closure like single-phase flows, but instead, starts rising slowly after the valve closure. With the rise of pressure, the vapor condenses and pressure oscillation begins after the condensation. For initial quality of 0.012 (test case 8), condensation occurs at ≈0.6 s after the valve closure. With higher initial quality of 0.025 (test case 9), condensation occurs at 2.2 s after the valve closure. Figure 8 shows the history of vapor quality (lower plot) and compressibility factor (upper plot) for test cases 8 and 9. It should be noted that the oscillation of compressibility factor begins after the condensation in both test cases.

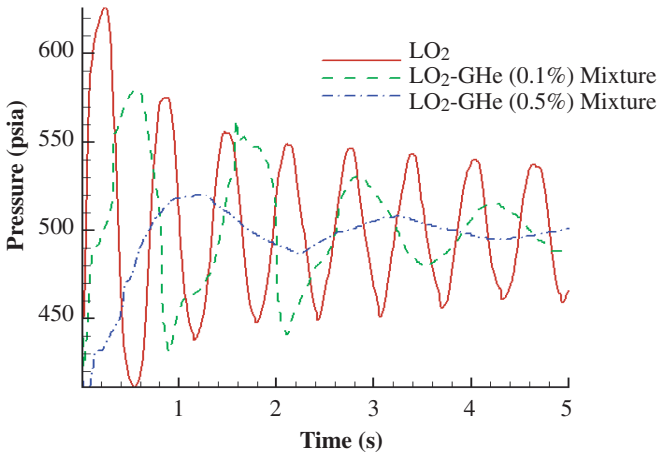

Figure 6. Comparison of predicted pressure history for liquid and gas-liquid mixtures (test cases 6 and 7).

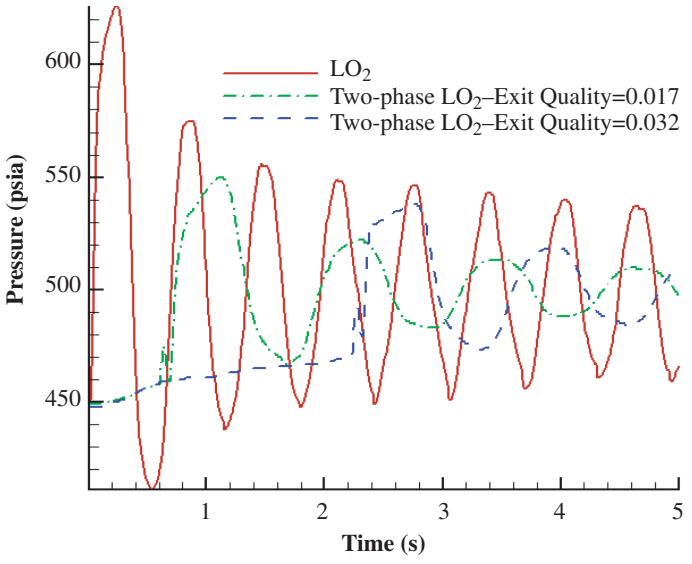

Figure 7. Predicted pressure oscillation due to condensation of LO_2 vapor following valve closure (test cases 8 and 9).

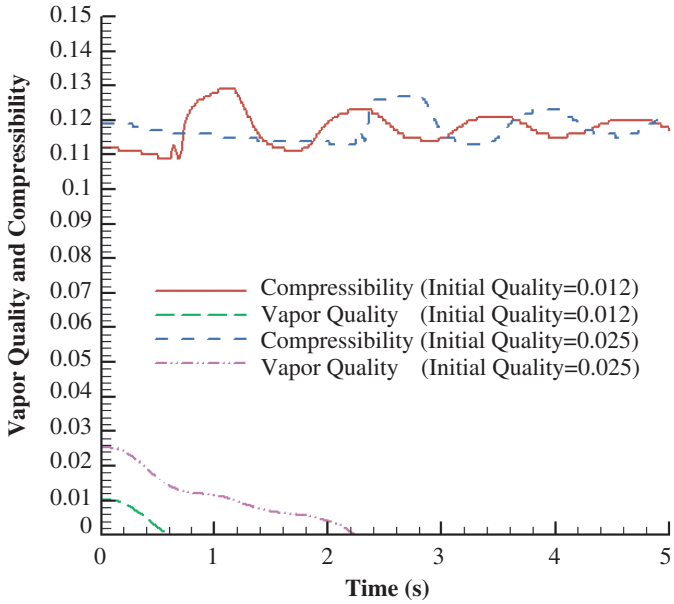

Figure 8. Predicted vapor quality and compressibility in test cases with condensation of LO_2 vapor (test cases 8 and 9).

Flow Circuit With Branching

Figure 1 shows a schematic of a propellant feed line (dotted line) connecting an LO_2 propellant tank operating at 500 psia and –260 °F with an isolation valve 400 ft downstream of the tank. The flow circuit also has an additional 400 ft of pipeline downstream of the valve and 240 ft of branch line upstream of the valve. The inner diameter of the pipeline, including branch line and tail pipe, is 0.25 in. Figure 9 shows the network model of this configuration. A steady-state flow distribution is first calculated with the given boundary pressures. The flowrate upstream of the branch is 0.097 lbm/s. After the branch, 0.0964 lbm/s flows through the isolation valve and 0.00052 lbm/s flows through the branch line. The valve located in branch 1112 closes in 0.1 s. The other two valves of the flow circuit (branch 2930 and 2223) were kept open during the period of simulation. The predicted pressure distributions in the upstream and downstream of the valve and in the branch line are shown in Figure 10. The predicted peak pressure is 15 psia less than test case 1. The observed reduction in peak pressure is due to flow branching. The present model, however, does not include the turning losses in the bend. The purpose of this test case is to demonstrate that the present procedure is capable of modeling the propagation of pressure surge in a parallel flow circuit.

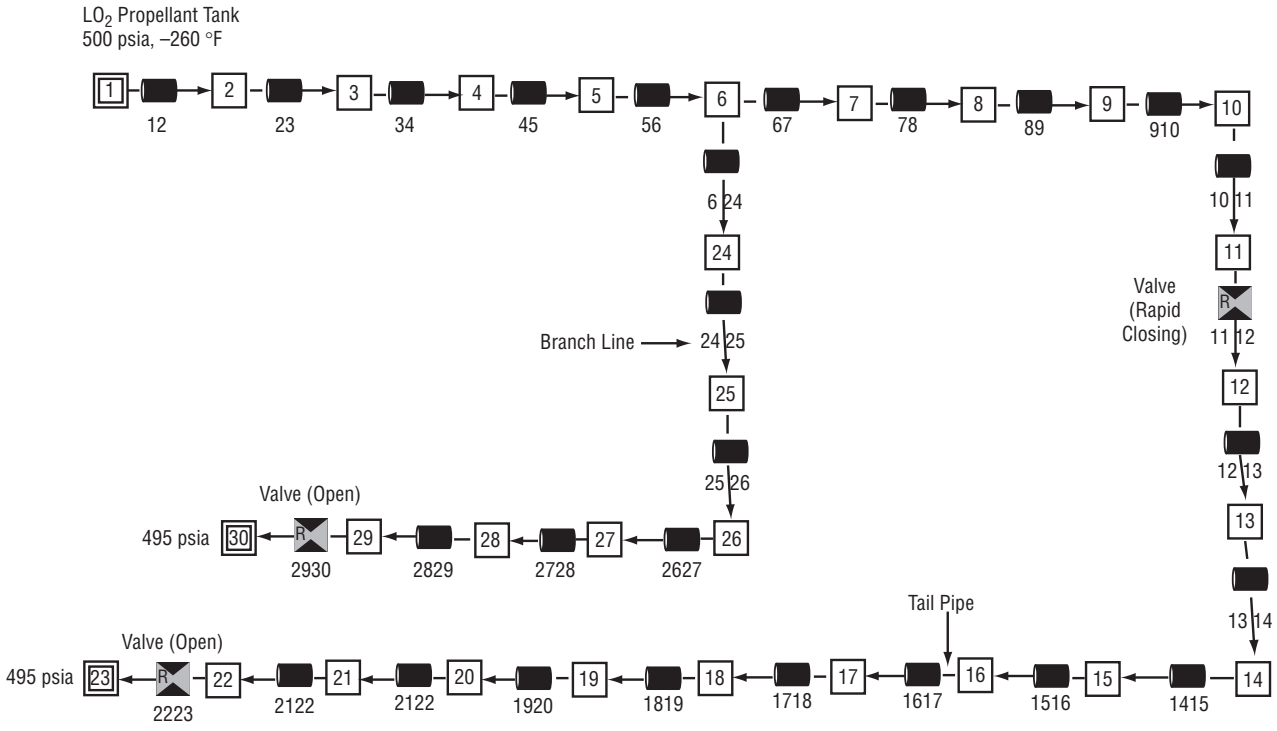

Figure 9. Finite volume model of the flow network with a branch line and a tail pipe.

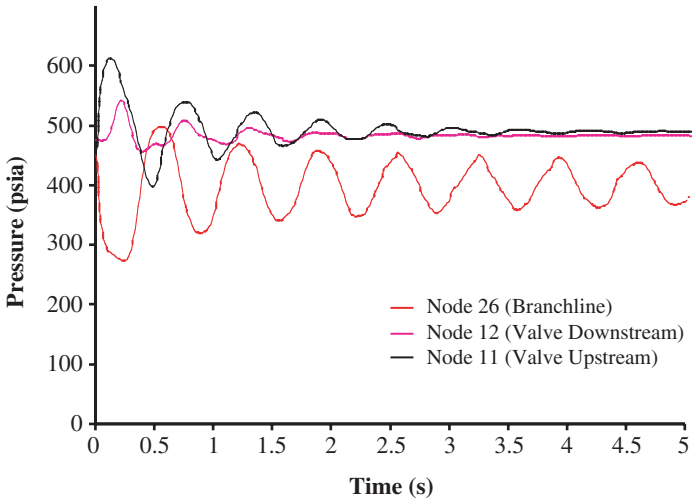

Figure 10. Predicted pressure history in flow circuit with branch following the valve closure (test cases 10).

CONCLUSIONS

A finite volume-based network flow analysis procedure has been extended to compute fluid transient following rapid valve closure. Liquid has been modeled as compressible fluid where the compressibility factor is computed from the equation of state for a real fluid. The modeling approach recognizes that the pressure oscillation is linked with the variation of the compressibility factor; therefore, the speed of sound does not explicitly appear in the governing equations. However, the finite volume solution has been verified by comparing it to the MOC solution of the governing equations that include the speed of sound. It has also been demonstrated that the present procedure can be applied to model fluid transients in a gas-liquid mixture and pressure oscillations due to condensation. The capability to predict fluid transient in a parallel flow circuit and tailpipe at downstream valves has also been demonstrated. However, additional test data and/or comparison to other methods will be required to validate these cases.

ACKNOWLEDGMENTS

This work has been performed under the MSFC Center Director's Discretionary Fund, Project No. 01–12. The authors would like to acknowledge Eric Stewart of the Thermodynamics and Heat Transfer Group (ED25), MSFC, for his comments and suggestions during the investigation, and the STI Publications Department of MSFC for preparation of the manuscript.

REFERENCES

1. Wylie, E. B., and Streeter, V., 1982, *Fluid Transients*, FEB Press, Ann Arbor, pp. 13–61.
2. Chaudhry, M. H., 1979, *Applied Hydraulic Transients*, Van Nostrand Reinhold Company, New York, pp. 44–73.
3. Moody, F. J., 1990, *Introduction to Unsteady Thermofluid Mechanics*, John Wiley & Sons, New York, pp. 408–422.
4. Chaudhry, M. H., and Hussaini, M. Y., "Second Order Explicit Finite Difference Methods for Transient Flow Analysis," Proceedings, *Numerical Methods for Fluid Transient Analysis*, ASME, FED – Vol. 4, Applied Mechanics, Bio-Engineering and Fluids Engineering Conference, June 20–22, 1983.
5. Majumdar, A. K., "A Second Law Based Unstructured Finite Volume Procedure for Generalized Flow Simulation," Paper No. AIAA 99–0934, 37th AIAA Aerospace Sciences Meeting Conference and Exhibit, Reno, NV, January 11–14, 1999.
6. Majumdar, A., November 1999, "Generalized Fluid System Simulation Program (GFSSP) Version 3.0," Report No. MG–99–290, Sverdrup Technology, Huntsville, AL.
7. Van Hooser, K., Bailey, J. W., and Majumdar, A. K., "Numerical Prediction of Transient Axial Thrust and Internal Flows in a Rocket Engine Turbopump," Paper No. 99–2189, 35th AIAA/ASME/SAE/ASEE Joint Propulsion Conference, Los Angeles, CA, June 20–24, 1999.
8. Majumdar, A. K., and Steadman, T., 2001, "Numerical Modeling of Pressurization of a Propellant Tank," *Journal of Propulsion and Power*, **17**(2), pp. 385–390.
9. Steadman, T., Majumdar, A. K., and Holt, K., "Numerical Modeling of Helium Pressurization System of Propulsion Test Article (PTA)," 10th Thermal Fluid Analysis Workshop, Huntsville, AL, September 13–17, 1999.
10. Cross, M. F., Majumdar, A. K., Bennett Jr., J. C., and Malla, R. B., 2002, "Modeling of Chill Down in Cryogenic Transfer Lines," *Journal of Spacecraft and Rockets*, **39**(2), pp. 284–289.
11. Patankar, S.V., 1980 *Numerical Heat Transfer*, Hemisphere Publishing Corp., Washington, DC.
12. Colebrook, C. F., 1938–1939, "Turbulent Flow in Pipes, with Particular Reference to the Transition Between the Smooth and Rough Pipe Laws," *J. Inst. Civil Engineering*, **11**, pp. 133–156.
13. Hendricks, R. C., Baron, A. K., and Peller, I. C., February 1975, "GASP—A Computer Code for Calculating the Thermodynamic and Transport Properties for Ten Fluids: Parahydrogen, Helium, Neon, Methane, Nitrogen, Carbon Monoxide, Oxygen, Fluorine, Argon, and Carbon Dioxide," *NASA TN D–7808*.
14. Hendricks, R. C., Peller, I. C., and Baron, A. K., November 1973, "WASP—A Flexible Fortran IV Computer Code for Calculating Water and Steam Properties," *NASA TN D–7391*.